Stiffer double-stranded DNA in two-dimensional confinement due to bending anisotropy

H. Salari
Department of Physics, Sharif University of Technology, P.O. Box 11155-9161, Tehran, Iran

B. Eslami-Mossallam
Department of Bionanoscience, Kavli Institute of Nanoscience, Delft University of Technology, Lorentzweg 1, 2628 CJ Delft, the Netherlands

H. F. Ranjbar
Institute of Complex Systems (ICS-2), Forschungszentrum Jülich, Wilhelm-Johnen-Straße, 52425 Jülich, Germany

M. R. Ejtehadi*
Department of Physics, Sharif University of Technology, P.O. Box 11155-9161, Tehran, Iran
and School of Nano Science, Institute for Research in Fundamental Sciences (IPM), Tehran 19395-5531, Iran
(Received 13 August 2016; published 19 December 2016)

Using analytical approach and Monte Carlo (MC) simulations, we study the elastic behavior of the intrinsically twisted elastic ribbons with bending anisotropy, such as double-stranded DNA (dsDNA), in two-dimensional (2D) confinement. We show that, due to the bending anisotropy, the persistence length of dsDNA in 2D conformations is always greater than three-dimensional (3D) conformations. This result is in consistence with the measured values for DNA persistence length in 2D and 3D in equal biological conditions. We also show that in two dimensions, an anisotropic, intrinsically twisted polymer exhibits an implicit twist-bend coupling, which leads to the transient curvature increasing with a half helical turn periodicity along the bent polymer.

DOI: 10.1103/PhysRevE.94.062407

I. INTRODUCTION

The bending flexibility of double-stranded DNA plays a crucial role in its interactions with other macromolecules, e.g., proteins. The most convenient measure of bending flexibility of a polymer is the "persistence length" (P), which is defined as the correlation length of the tangent unit vector along the contour length [1]. Many experimental and simulational techniques have been performed to measure this quantity of the DNA molecule [2–16] and characterize its dependence on the ionic strength [3,5,13,17], temperature [10], sequence [18], and length scale [19–21]. In the single-molecule stretching experiment, Baumann *et al.* have shown that the persistence length of a random DNA sequence in moderate salt buffer is around 45–50 nm [3]. Other bulk experiments, such as DNA cyclization [6,18] and gel electrophoretic mobility [5,22], also result in a value in this range (Table I).

On the other hand, single-molecule imaging techniques, including atomic force microscopy (AFM) and electron microscopy (EM), introduce an important new class of experiments to measure the persistence length of DNA molecule. In these experiments the molecules are attracted onto the surface of a substrate by divalent counterions, e.g., Mg^{2+} [15,23]. These divalent ions allow the molecule freely equilibrate in two dimensions and decrease the effects of the substrate on the chain statistics [9]. It is also known that a small amount of Mg^{2+} in solution can dramatically decrease the persistence length [3,4]. Baumann *et al.* show that, with 0.1 mM of Mg^{2+}, even with a small amount of monovalent counterions (e.g., 1.86 mM Na^{+}), the persistence length of DNA decreases to 40.9 ± 3.7 nm [3]. However, the DNA persistence length measured in 2D, P_{2D} [7–9,11–13,15,16], is generally bigger than the three-dimensional (3D) values, P_{3D} [2–6,10,14], in the presence of divalent counterions (see Fig. 1). There are two experiments which do not address this discrepancy between two-dimensional (2D) and 3D persistence lengths of dsDNA [24,25]. In these works different buffers were used in the 2D and 3D experiments, where Mg^{2+} is present only in the 2D experiment buffer. Thus, they are not shown in Fig. 1. According to Fig. 1, the average value of P_{2D} is about 55.8 ± 3.5 nm and remains almost constant with increasing the ionic strengths in contrast to P_{3D}, which drops slowly.

This visible difference may arise from different effects of the divalent counterions within the experiments, i.e., measuring the persistence length in 2D and 3D conformations. It is known that in two dimensions, the divalent counterions bridge the negative charges of the phosphate backbone to the negatively charged mica surface [15,24], while they act as intramolecular bridges between two phosphates in 3D conformations [30]. The bridges in the latter can greatly reduce the entropy of the chain and lead to low persistence lengths. In addition, the excluded volume interactions in 2D conformations can swell the molecule and therefore increase the persistence length [15,31,32]. Rivetti *et al.* show that, although these interactions can increase the 2D persistence length, this effect is negligible when DNA length is less than 1000 nm ($\simeq$3400 bp) [15]. But the molecules in two dimensions remain stiffer, even for lengths shorter than 3400 bp [8,9,12,13,15,16]. Moreover, transition from B-DNA to A-DNA during the imaging in the dry air can also make DNA stiffer [33–36]. To avoid this structural transition, DNA molecules in Fig. 1 were scanned in solution and biological conditions. Also, the errors in contour length estimation can affect the measured values for the persistence length. Underestimating by $\sim$2% leads to about $\sim$60% overestimation

*ejtehadi@sharif.edu

TABLE I. Some reported values of the persistence length of dsDNA measured by various techniques in 3D conformations.

Buffer composition	Method	$P_{(3D)}$ (nm)	Ref.
10 mM Na^+, pH 7.0, 25 °C	DE[a]	47.4 ± 1.0	[2]
93.0 mM Na^+, pH 7.0, 25 °C	DE	43.8 ± 1.4	[3]
10 mM Na^+	DE	50	[26]
200 mM K^+, 10 mM Tris-HC1, pH 7.2, 25 °C	LS[b]	48 ± 1	[27]
100 mM Na^+, 20 °C	LS	45	[28]
110 mM Na^+, pH 7.4, 25 °C	TPM[c]	47.8 ± 0.7	[4]
100 mM Na^+, 20 °C	FD[d]	48	[22]
101 mM Na^+, 20 °C	TED[e]	44	[5]
0-162 mM Na^+, 1 mM Mg^{2+}, pH 7.8, 16 °C	DC[f]	45.0 ± 1.5	[6]
89 mM Tris borate/2 mM EDTA, pH 8.3	DC	48.5	[18]
Moderate salt buffer	Cryo-EM[g]	45	[29]

[a]DNA stretching
[b]Light scattering
[c]Tethered particle motion
[d]Flow dichroism
[e]Transient electric dichroism
[f]DNA cyclization
[g]Cryo-electron microscopy

of P_{2D} for a 100 bp DNA [37]. But this effect is reduced by increasing the contour length, where the overestimation decreases to ∼10% for a 500 bp DNA [37]. Finally, it has been also mentioned that the surface charges can affect the flexibility of DNA [13]. Apart from above possibilities here we show that the anisotropic bending tendency of double-stranded DNA (dsDNA) increases the stiffness of the molecule in two dimensions.

The anisotropic bending of (dsDNA) is a property of the sugar-phosphate backbone structure, in the sense that bending toward the grooves direction (roll) is much easier than toward the backbone direction (tilt) [38]. Fourier analysis of free energy of DNA loops with lengths between 60–100 bp shows two main oscillatory components [39]: one with a helical period (∼10.5 bp) and another with a half helical period (∼5.6 bp) which may reflect the bending anisotropy. The sequence-dependent bending anisotropy of B-DNA has been observed in x-ray crystallography of DNA-protein complexes [40,41] and NMR spectroscopy [42], as well as all-atomistic simulations [43–50]. Many theoretical studies have considered such anisotropic bending into the elastic models [51–57], and it is shown that although the bending anisotropy affect the elastic properties of a short DNA molecule in three dimensions, it becomes unimportant when the DNA segment is long enough to include a few full helical turns [54,58].

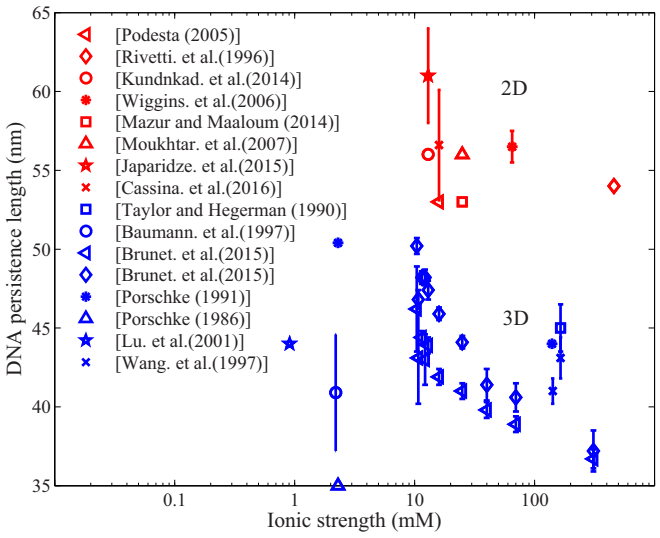

FIG. 1. Comparison between the reported values of P_{2D} (red dots) and P_{3D} (blue dots) for different ionic strength in the presence of divalent counter-ions. The ionic strength is defined as Ref. [4], and different markers correspond to different references as indicated in the legend.

Here we exploit methods from the statistical field theory as well as Monte Carlo simulation technique to study the elastic properties of an intrinsically twisted ribbon with anisotropic bending in two dimensions. We show that it is possible to assign an effective persistence length to a long DNA molecule in two dimensions, similar to the 3D case. Whereas the isotropic bending model predicts equal persistence lengths in two and three dimensions, we show that due to the anisotropic bending the 2D persistence length is always bigger than the one in three dimensions. The difference between 2D and 3D persistence lengths depends on the relative strengths of the bending elastic constants (the strength of anisotropy) and also twist rigidity, while the latter implies an implicit twist-bend coupling in the model. The prediction of our model for the DNA persistence length in two dimensions is in good agreement with the experimental data, shown in Fig. 1. Our finding can be relevant to other anisotropic chain polymers, e.g., double-stranded RNA or carbon nanoribbons [59].

II. MODEL AND MATERIALS

A. The planar anisotropic elastic rod model

Double-stranded DNA is a helical nanoribbon polymer which is represented as an anisotropic elastic rod. As Fig. 2 shows, at each point of arc length parameter s on the centerline, $\vec{r}(s)$, one can attach an orthonormal basis $\{\hat{d}_1,\hat{d}_2,\hat{d}_3\}$, a so-called "material frame." There are the two usual definitions

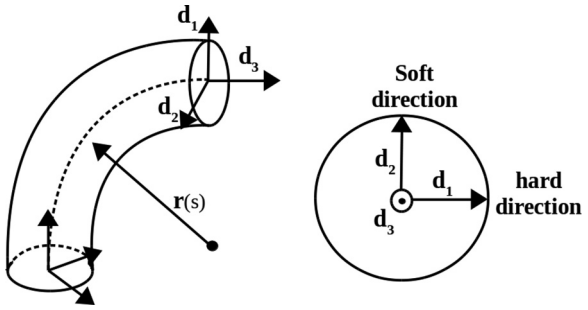

FIG. 2. Parametrization of the elastic rod.

for $\hat{d}_3$ [19], but in the simplest way it can be chosen to be along the tangent to the rod at every point so that $\hat{d}_3(s) = \hat{t}(s) \equiv (d/ds)\vec{r}(s)$ [60]. $\hat{d}_1$ is along the grooves direction and points toward the major groove, and $\hat{d}_2 = \hat{d}_3 \times \hat{d}_1$. Here we assume bending about the $\hat{d}_2$ axis is easer than the $\hat{d}_1$ axis, therefore, the $\hat{d}_1$ and $\hat{d}_2$ axes correspond to the hard and soft bending directions (see Fig. 2).

The derivatives of the orthonormal triads with respect to s are defined as

$$\dot{\hat{d}}_i \equiv \frac{d}{ds}\hat{d}_i = \mathbf{\Omega} \times \hat{d}_i, \quad i = 1,2,3, \tag{1}$$

where $\mathbf{\Omega}(s) = \kappa_1\hat{d}_1 + \kappa_2\hat{d}_2 + \omega\hat{d}_3$ is called the strain vector. The components of $\mathbf{\Omega}$ (i.e., κ_1,κ_2, and ω) respectively correspond to rotation of the filament around $\hat{d}_1$, $\hat{d}_2$, and $\hat{d}_3$ and called tilt, roll, and twist [21]. Therefore, the elastic energy of an inextensible, unshearable, and anisotropic filament in harmonic approximation can be written as [54,56]

$$E/k_BT = 1/2\int_0^L ds\left[A_1\kappa_1^2 + A_2\kappa_2^2 + C(\omega - \omega_0)^2\right], \tag{2}$$

where A_1 and A_2 are bending rigidities, respectively, for the hard and soft directions, C is the twist rigidity, and $\omega_0 = 1.8\ \mathrm{nm}^{-1}$ is intrinsic twist of B-DNA. In the elastic energy of Eq. (2), we have ignored the explicit twist-bend coupling [61–63].

For a planar DNA (confined in the x-y plane where $\hat{z}.\hat{d}_3 = 0$), it is convenient to express the local triads in terms of Euler angles $\mathbf{\Theta}(s) = [\alpha(s),\beta(s),\psi(s)]$ $(0 < \alpha < 2\pi,\ \beta(s) = \pi/2,\ 0 < \psi < 2\pi)$ as [54]

$$\begin{aligned}
\hat{d}_1(s) &= -\sin\psi\sin\alpha\,\hat{x} + \sin\psi\cos\alpha\,\hat{y} + \cos\psi\,\hat{z},\\
\hat{d}_2(s) &= -\cos\psi\sin\alpha\,\hat{x} + \cos\psi\cos\alpha\,\hat{y} - \sin\psi\,\hat{z},\\
\hat{d}_3(s) &= \cos\alpha\,\hat{x} + \sin\alpha\,\hat{y},
\end{aligned} \tag{3}$$

where $\alpha(s)$ and $\psi(s)$, respectively, correspond to the local bend and twist angles. By substituting Eq. (3) into Eq. (1) one can obtain the components of $\mathbf{\Omega}$,

$$\begin{aligned}
\kappa_1(s) &= \dot{\alpha}(s)\cos\psi(s),\\
\kappa_2(s) &= \dot{\alpha}(s)\sin\psi(s),\\
\omega(s) &= \dot{\psi}(s),
\end{aligned} \tag{4}$$

and the local curvature is $\kappa(s) = \sqrt{\kappa_1^2 + \kappa_2^2} = \dot{\alpha}$.

Experimentally, the persistence length of DNA in a 2D conformation can be determined by measuring various statistical properties, such as the orientational correlation function [24,64], the probability distribution of the bending angle [11,16], the mean-square end-to-end distance [12,15,23,30], and force extension [65]. The isotropic wormlike chain (WLC) model, i.e., $A_1 = A_2 = P$, has been widely used to fit the experimental data and obtain the persistence length. Below we derive each of these statistical properties for an anisotropic elastic model, where $A_1 > A_2$.

For a chain with length L and global bend angle $\theta(L)$ $(= \int_0^L \kappa(s)ds)$ in two dimensions the free energy is given by the canonical relation [66,67]:

$$F[\theta(L)] = -k_BT\ln\{p_{2D}[\theta(L)]\}, \tag{5}$$

where $p[\theta(L)]_{2D}$ is the normalized probability distribution of θ for 2D conformation. This probability distribution can be written as a path integral

$$\begin{aligned}
p_{2D}[\theta(L)] = \mathcal{N}\int \mathcal{D}[\mathbf{\Theta}]\exp\left[-\int_0^L \frac{e[\mathbf{\Theta}(s)]}{k_BT}\,ds\right]\\
\times\delta\left[\theta - \int_0^L \kappa(s)\,ds\right],
\end{aligned} \tag{6}$$

where $\mathcal{N}$ is the normalization constant and

$$\frac{e[\mathbf{\Theta}(s)]}{k_BT} = \frac{1}{2}(A_1\cos^2\psi + A_2\sin^2\psi)\dot{\alpha}^2 + \frac{1}{2}C(\dot{\psi} - \omega_0)^2 \tag{7}$$

is the density of elastic energy. In the case of the isotropic WLC model, $p_{2D}[\theta(L)]$ follows a Gaussian distribution as $\sqrt{2P/\pi L}\exp(-P\theta^2/2L)$, but in general, due to the first term of the right-hand side of Eq. (7), it is not easy to find an expression for $p_{2D}[\theta(L)]$. Using the probability distribution (6), the tangent-tangent correlation function, $\langle\hat{d}_3(L)\hat{d}_3(0)\rangle_{2D} = \langle\cos[\theta(L)]\rangle_{2D}$, as a function of L is defined as [15]

$$\langle\cos[\theta(L)]\rangle_{2D} \equiv \int_0^{+\infty} d\theta\cos[\theta(L)]p_{(2D)}[\theta(L)], \tag{8}$$

where we suppose that $\theta \geqslant 0$. It can be easily shown that for the isotropic case we have $\langle\cos[\theta(L)]\rangle_{2D} = \exp(-L/2P)$. Finally, the mean-squared end-to-end distance of the chain for short lengths, where the excluded volume interactions are negligible [32], is written by

$$\begin{aligned}
\langle R^2\rangle_{2D} &= \int_0^L\int_0^L \langle\hat{d}_3(s)\,\hat{d}_3(s')\rangle_{2D}\,ds\,ds'\\
&= \int_0^L\int_0^L \langle\cos(\theta(s - s')\rangle_{2D}\,ds\,ds',
\end{aligned} \tag{9}$$

where $\theta(s - s')$ is the angle between tangent vectors at points s and s' along the contour. The above equation for the isotropic model can be directly determined by substituting $\langle\cos[\theta(s - s')]\rangle_{2D} = \exp[-(s - s')/2P]$ and straightforward integration as [68]

$$\langle R^2\rangle_{2D} = 4PL - 8P^2\left[1 - \exp\left(\frac{-L}{2P}\right)\right]. \tag{10}$$

In the case of an anisotropic elastic model the first term of the right-hand side of Eq. (7) implies an implicit twist-bending coupling for the model. In order to find the effects of this coupling, we evaluate $p_{2D}[\theta(L)]$ in two extreme limits: the large and small twist rigidity (i.e., $C \to \infty$ and $C \to 0$, respectively).

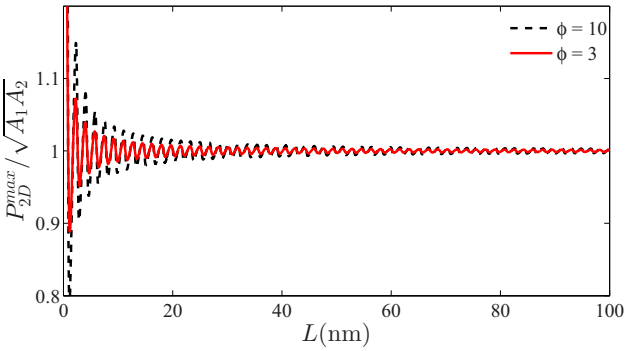

FIG. 3. The ratio of $P_{2D}^{\max}/\sqrt{A_1A_2}$ (Eq. (14)) as a function of length for two different values of ϕ and $\psi_0 = 0$.

For large twist rigidity, the relative variations of $\dot{\psi}$ is negligible and $\dot{\psi} \simeq \omega_0$, which gives $\psi = \omega_0 s + \psi_0$, where ψ_0 is the initial twist angle. Therefore, the density of energy (7) reduces to

$$e_\infty[\kappa(s)]/k_BT = \tfrac{1}{2}\tilde{A}(\omega_0 s + \psi_0)\kappa(s)^2, \tag{11}$$

where $\tilde{A}(\omega_0 s + \psi_0) = A_1\cos^2(\omega_0 s + \psi_0) + A_2\sin^2(\omega_0 s + \psi_0)$. By substituting this energy density into Eq. (6) and replacing the Dirac delta function by the appropriate Fourier transform, one can find the probability distribution of $p_{2D}(\theta(L))$ as

$$p_{2D}[\theta(L)] = \mathcal{N}\int_{-\infty}^{+\infty}\frac{dK}{2\pi}e^{iK\theta}\int\mathcal{D}[\kappa] \times \exp\left\{-\int_0^L\left[\frac{\tilde{A}(\omega_0 s+\psi_0)}{2}\kappa^2 + iK\kappa\right]ds\right\}. \tag{12}$$

Then, upon a straightforward integration, this equation yields a Gaussian distribution

$$p_{2D}[\theta(L)] = \sqrt{\frac{2P_{2D}^{\max}}{\pi L}} \times \exp\left(-\frac{P_{2D}^{\max}\theta^2}{2L}\right) \tag{13}$$

with

$$\frac{1}{P_{2D}^{\max}} = \frac{1}{L}\int_0^L\frac{ds}{\tilde{A}(\omega_0 s+\psi_0)} = \frac{\mathcal{Y}(L\omega_0+\psi_0)-\mathcal{Y}(\psi_0)}{L\omega_0\sqrt{A_1A_2}}, \tag{14}$$

where

$$\mathcal{Y}(x) = \tan^{-1}[\phi^{-1/2}\tan(x)] + \pi\left[\left[\frac{1}{2}+\frac{x}{\pi}\right]\right], \tag{15}$$

and $\phi = A_1/A_2$. The double brackets mean "integer part," which is added to get rid of discontinuity in the $\tan^{-1}$ function. Figure 3 indicates the length dependence of $P_{2D}^{\max}/\sqrt{A_1A_2}$ for $\psi_0 = 0$ and two different values of ϕ. It can be shown that by increasing the chain length, $P_{2D}^{\max}$ soon approaches its asymptotic value $\sqrt{A_1A_2}$ [71] for any value of ψ_0, and then

$$P_{2D}^{\max} = \sqrt{A_1A_2} \quad \text{for} \quad L\omega_0 \gg 1, \tag{16}$$

which implies that at large twist rigidity limit, a long enough 2D anisotropic DNA behaves like an isotropic DNA with the bending constant $\sqrt{A_1A_2}$.

On the other hand, in the limiting case of the small twist rigidity, there is no constraint on the twist degree of freedom, and then the local twist angle, $\psi(s)$, is free to choose any value in the range $[0,2\pi]$. The distribution of ψ for an unconstrained chain is uniform due to temperature and entropy. But under additional external constraints it would change. Therefore, the energy density of (7) in this limit is rewritten as

$$e_0[\kappa,\psi]/k_BT = \tfrac{1}{2}\tilde{A}(\psi)\kappa^2. \tag{17}$$

Substituting this equation into Eq. (6), one can find $p_{2D}[\theta(L)]$, in this limit, as

$$p_{2D}[\theta(L)] = \mathcal{N}\int_{-\infty}^{+\infty}\frac{dK}{2\pi}e^{iK\theta}\int\mathcal{D}[\kappa]\mathcal{D}[\psi] \times \exp\left\{-\int_0^L\left[\frac{\tilde{A}(\psi)}{2}\kappa^2 + iK\kappa\right]ds\right\} = \sqrt{\frac{2P_{2D}^{\min}}{\pi L}} \times \exp\left(-\frac{P_{2D}^{\min}\theta^2}{2L}\right), \tag{18}$$

where

$$P_{2D}^{\min} = \frac{\int_0^{2\pi}d\psi/\tilde{A}(\psi)^{1/2}}{\int_0^{2\pi}d\psi/\tilde{A}(\psi)^{3/2}}. \tag{19}$$

We numerically solve this equation for any given A_1 and A_2 in the rest of this work.

From Eqs. (13) and (18), it can be deduced that the anisotropic elastic model in 2D behaves like a isotropic model with an effective persistence length, P_{2D}, which is a function of A_1, A_2, C, and $\omega_0 L$. As P_{2D} varies by the strength of twist rigidity, the upper and lower limits of P_{2D} are given by $P_{2D}^{\max}$ [Eq. (14)] and $P_{2D}^{\min}$ [Eq. (19)], respectively. We perform Monte Carlo simulations to evaluate P_{2D} between these two extreme limits.

B. Monte Carlo simulations

To calculate the statistical properties of the chain, we performed Metropolis Monte Carlo (MC) simulations of a discrete elastic model from Eq. (2) at the base pair level same as in Ref. [21]. Here the chain consists of beads were connected to adjacent beads via a link length 0.34 nm and without excluded volume interactions (a phantom chain). We used the pivot, twist, and crankshaft (just in 3D simulations) moves with appropriate Boltzmann distributions to construct equilibrium configurations of the chain. Our simulations were done with a linear chain containing 600 beads in 2D and 3D conformations, and each bead has an equal chance to move during the simulations.

We start with a random initial condition, and the first 10^5 MC steps were discarded to ensure the equilibration of the system and the next 10^7 MC steps were considered for sampling. To estimate the statistical errors, we performed five realizations with different initial conditions. Figure 4 shows the typical configurations of the chain in 3D and 2D states that are obtained by the MC simulations.

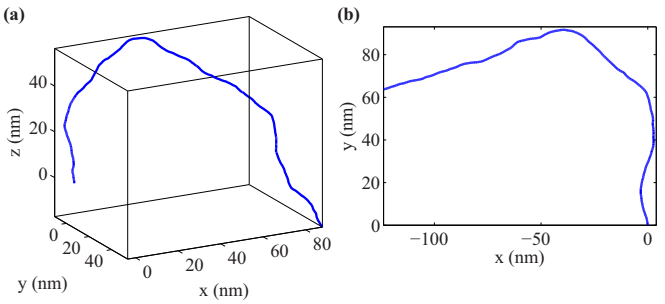

FIG. 4. The typical configurations of the chain in 3D (a) and 2D (b) states.

III. RESULTS AND DISCUSSION

A. The elastic properties of the long anisotropic chain

Similar to experiments [9,15,64], we used the tangent-tangent correlation function as well as the mean square of end-to-end distance to extract the effective persistence length of a long chain from the MC simulations. To address the effects of 2D confinement on the flexibility of chain, we compare the effective persistence length in both 2D and 3D conformations.

It is well known that the tangent-tangent correlation function of a free, long, and highly twisted anisotropic model in three dimensions decays as $\langle \cos\theta(L)\rangle_{3D} = \exp(-L/P_{3D})$, where P_{3D} is given by the harmonic mean of the hard and soft bending rigidities, A_1 and A_2 [46,54,69]:

$$P_{3D} = 2(1/A_1 + 1/A_2)^{-1}. \tag{20}$$

Figure 5(a) compares the MC results of the 3D correlation function, $\langle \cos\theta(L)\rangle_{3D}$, for the chains with $A_1 = 275$ nm and $A_2 = 27.5$ nm (i.e.m $\phi = 10$) and three different values of C, i.e., 0.1 (open blue squares), 5 (open green circles), and 100 nm (open red triangles). P_{3D} is determined by the slope of the best fitted lines to $-L/\ln\langle \cos\theta(L)\rangle_{3D}$ (the solid lines). As can be seen from the inset of Fig. 5(a), P_{3D} is independent on C and equal to the harmonic mean of A_1 and A_2 (i.e., 50 nm, dashed line). Figure 5(b) shows the correlation function in two dimensions, $\langle \cos\theta(L)\rangle_{2D} = \exp(-L/2P_{2D})$; here a clear dependence on C is evident. We found that P_{2D} is always greater than P_{3D} [dashed line in the inset of Fig. 5(b)] and varies from $P_{2D}^{\min} = 64.2$ nm for $C = 0.1$ nm to $P_{2D}^{\max} = 87.0$ nm for $C = 100$ nm [the solid lines in the inset of Fig. 5(b)]. Since the zero-energy configuration of a curved anisotropic chain is not planar [56], then it takes energy to enforce the chain in 2D confinement. This extra energy makes the chain stiffer in two than three dimensions.

All sets of A_1 and A_2 result in the same P_{3D}, but different ϕ values are given by

$$\begin{aligned} A_1 &= P_{3D}/(1-\lambda), \\ A_2 &= P_{3D}/(1+\lambda), \end{aligned} \tag{21}$$

where $\lambda = \frac{\phi-1}{\phi+1}$. Therefore, it is convenient to consider P_{2D} as a function of P_{3D}, ϕ, and C. Figure 6 shows a fairly linear relationship between P_{2D} and P_{3D} for different values of ϕ and C. We therefore expect that the ratio P_{2D}/P_{3D} is independent of P_{3D}. Figure 7 shows the dependence of this ratio on ϕ and C. As Fig. 7(a) indicates, P_{2D} is always greater than P_{3D} when

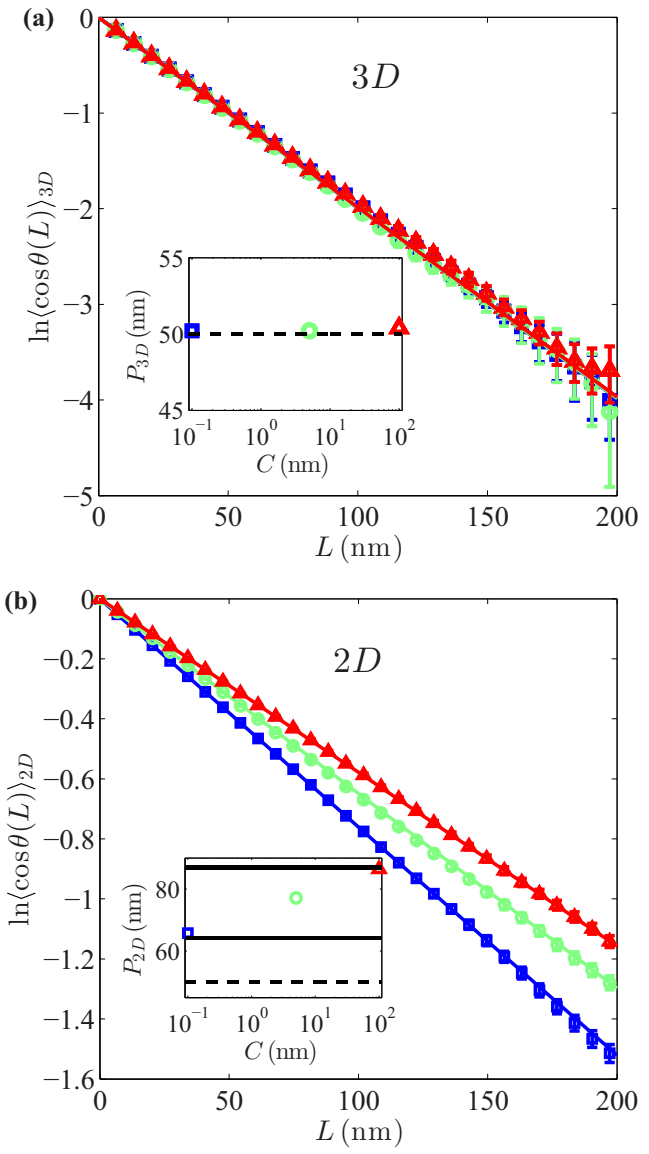

FIG. 5. The MC results for the tangent-tangent correlation function in 3D (a) and 2D (b) for $A_1 = 275$ nm, $A_2 = 27.5$ nm with a harmonic mean of 50 nm (dashed lines in the insets). The data points correspond to $C = 0.1$ (open, blue squares), 5 (open, green circles), and 100 nm (open, red triangles), and the straight lines indicate linear fits to data. The insets show the measured persistence lengths from the slope of the fitted lines (see text). The solid lines, in the inset of panel (b), correspond to the upper (87.0 nm) and lower (64.2 nm) limits of P_{2D} versus C [Eqs. (16) and (19), respectively].

$\phi \neq 1$ (i.e., anisotropic bending), and they are equal at $\phi = 1$ (i.e., isotropic bending). It can be seen that P_{2D} as well as its lower and upper limits $P_{2D}^{\min}$ and $P_{2D}^{\max}$ increase with ϕ. The twist-bend coupling which is reflected in the dependence of P_{2D} on C also becomes stronger with increasing ϕ. As Fig. 7(b) shows, P_{2D} strongly depends on the twist rigidity, C, in the range 1–30 nm (the region between two vertical dashed line) and beyond that is approximately constant and given by $P_{2D}^{\max}$ [Eq. (16)] and $P_{2D}^{\min}$ [Eq. (19)] for $C \gtrsim 30$ nm and $C \lesssim 1$ nm, respectively.

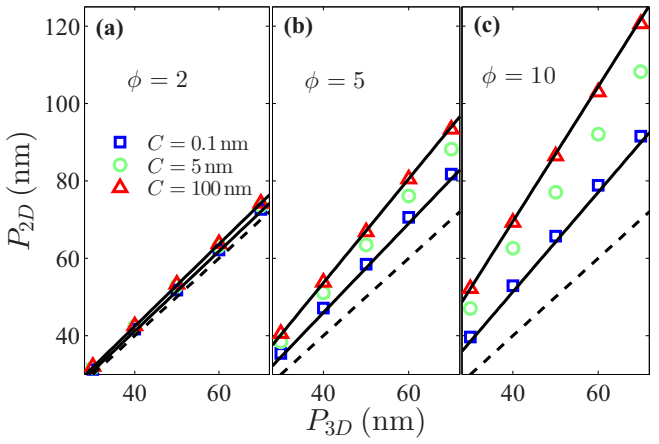

FIG. 6. The dependence of P_{2D} on P_{3D} for different values of C and ϕ, as indicated. Solid lines correspond to the upper and lower limits of P_{2D} (i.e., P_{2D}^{max} and P_{2D}^{min}, respectively), and dashed lines are with slope equal to 1. Error bars (not shown) are about the size of the markers.

Another way to calculate the persistence length is based on the mean-square of end-to-end distance $\langle R^2\rangle_{2D}$. Figure 8 shows the MC results of $\langle R^2\rangle_{2D}$ lie perfectly on the predictions of Eq. (10), where P_{2D} is substituting from Fig. 5(b). It means that the persistence lengths which are extracted from the mean-square of end-to-end distance are very close to those calculated from the tangent-tangent correlation function, and the relative error between these two is less than 1%.

B. Stretching anisotropic chain in two dimensions

We also studied the entropic stretching of the anisotropic chain in response of an external force in two dimensions using MC simulations. The external potential $U = -fx$ is added to the the elastic energy [Eq. (2)], where f is the magnitude of the external force which is exerted on the last bead of the chain, and x is the component of the end-to-end vector in the direction of the external force. It is known that the force versus extension curve of an isotropic chain (i.e., $A_1 = A_2 = P$) in two dimensions is given by [70]

$$fP/k_BT = \frac{1}{16}\left[6\frac{\langle x\rangle}{L} - 1 + \left(1 - \frac{\langle x\rangle}{L}\right)^{-2}\right], \qquad (22)$$

where $\langle x\rangle$ is the average extension along the force direction. Figure 9 shows the 2D force-extension curve for the chains with $L = 204$ nm, $C = 100$ nm, $P_{3D} = 50$ nm, and different values of ϕ: 1 (open blue circles), 3 (open green triangles), 6 (open red squares), and 10 (open black triangles). As can be seen, each set of force-extension data perfectly lies on the theoretical prediction of Eq. (22) (solid curve), when the external force is scaled by its corresponding P_{2D} [extracted from Fig. 7(b)]. This shows the force-extension characteristic of an anisotropic chain is same as an isotropic chain with the appropriate persistence length of P_{2D}.

C. The elasticity of the anisotropic chain at small length scales

To investigate the flexibility of the anisotropic model at short length scales, we computed the negative logarithm of the probability distribution of bending angle, $-\ln\{p_{2D}[\theta(L)]\}$. Figure 10 shows the result for 10.2 nm chain with $P_{3D} = 50$ nm, $\phi = 10$, and $C = 0.1$, 1.4, and 55 nm. The effective persistence length of the chain at this length can be extracted by fitting a parabola of the form $(P_{2D}/2L)\theta^2 + \text{const}$ to the data (see the inset of Fig. 10) and is in good agreement with our previous result [see Fig 5(b)]. It can be seen in Fig. 10 that the large bending appears to be easier than the expected from the theory in $C = 1.4$ and $C = 0.1$. It means for small values of C (<30 nm) there is no guarantee that the bending free energy is a parabola.

Due to the intrinsic helicity and bending anisotropy of the DNA molecule, we expect that the effective persistence length at small length scales oscillates with a period of $\pi/\omega_0 \backsimeq 1.7$ nm. Using $-\ln\{p_{2D}[\theta(L)]\}$ we calculate P_{2D} for the

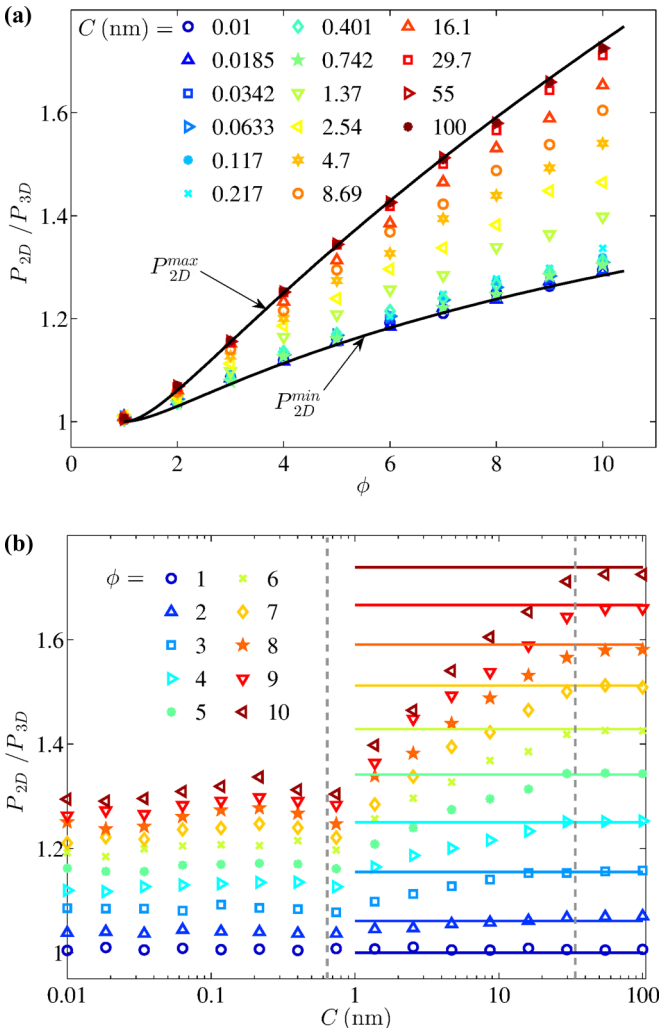

FIG. 7. (a) Dependence of P_{2D}/P_{3D} on ϕ for different values of C in the range 0.01–100 nm (from dark blue to dark red). The solid curves correspond to theoretical predictions for P_{2D}^{min} (when $C \to 0$) and P_{2D}^{max} (when $C \to \infty$). (b) Dependence of P_{2D}/P_{3D} on C for different values of ϕ. The horizontal solid lines indicate the value of P_{2D}^{max} for the corresponding ϕ, and the region between the vertical dashed (gray) lines indicates the region with strong twist-bend coupling regime. Error bars (not shown) are about the size of the markers.

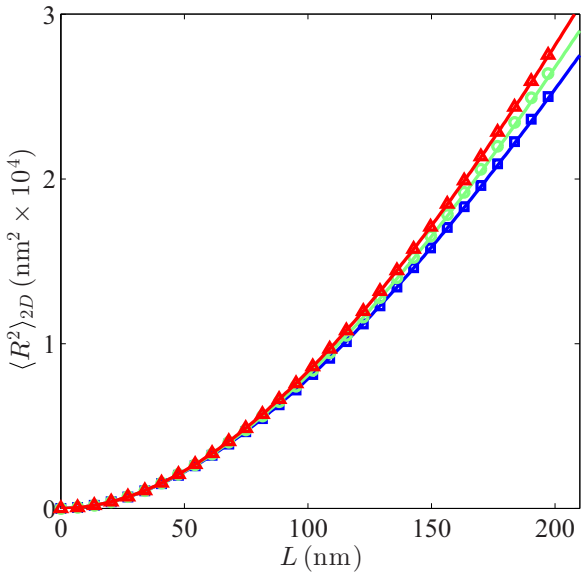

FIG. 8. The mean-square of end-to-end distance $\langle R^2\rangle_{2D}$ versus the chain length L. The data points correspond to the MC simulations of chains with $P_{3D} = 50$ nm, $\phi = 10$, and different values of C (same as Fig. 5), and the solid curves are the predictions. Error bars (not shown) are about the size of the markers.

segment lengths between 1.7 and 6.8 nm. Figure 11 compares the MC results (the squares) and theoretical predictions (solid, red line) of the ratio $P_{2D}/\sqrt{A_1A_2}$ for $C = 100$ nm and different values of $\phi = 1$, 3, 5, 7, and 9. The theoretical predictions are obtained by taking average of Eq. (14) over $0 \leqslant \psi_0 \leqslant 2\pi$, because the initial value of twist angle, ψ_0, can be changed during the simulation procedure. It can be seen that P_{2D} oscillates with a period of about 1.7 nm and decays to its extreme value of $\sqrt{A_1A_2} = P_{3D}/\sqrt{1-\lambda^2}$ by increasing the

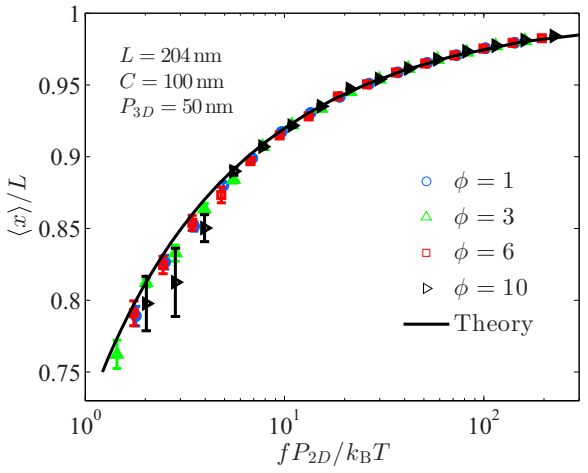

FIG. 9. Semilogarithmic plot of the relative extension, $\langle x\rangle/L$, versus the scaled force, fP_{2D}/k_BT, for the anisotropic chains with $L = 204$ nm, $C = 100$ nm, $P_{3D} = 50$ nm, and different values of ϕ (as indicated) in two dimensions. P_{2D} for each set of data was extracted from Fig, 7(b). The solid curve corresponds to the theoretical prediction of Eq. (22).

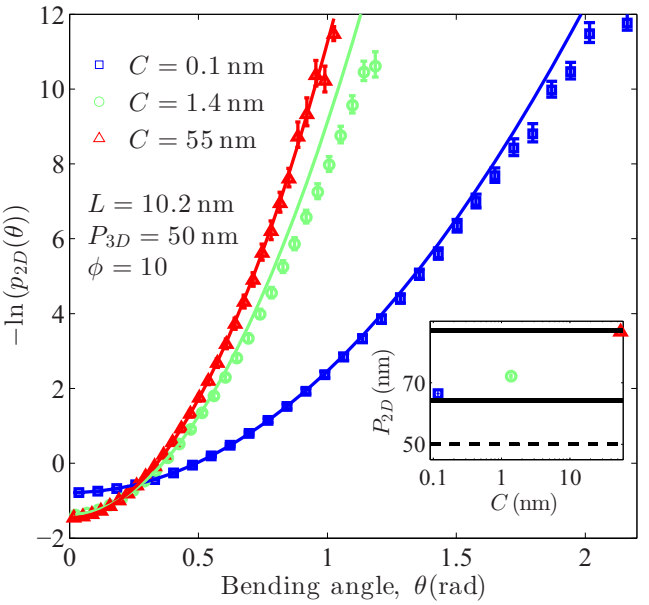

FIG. 10. The probability distribution $p_{2D}(\theta)$ for the angle θ between tangents of two points separated by a contour length of $L = 10.2$ nm. The data points correspond to MC simulations of the chains with $P_{3D} = 50$ nm, $\phi = 10$, and three different values of C, as indicated. Solid curves are the best parabolic fits to the data. Inset: Semilogarithmic plot of P_{2D} versus C. The solid (black) lines correspond to the upper (i.e., P_{2D}^{max}) and lower (i.e., P_{2D}^{min}) limits of P_{2D}, and the dashed line indicates P_{3D}.

length. This oscillation is amplified if the strength of bending anisotropy, ϕ, increases.

The oscillations are due to the formation of transient curvature increasing with periodic arrangement in 2D

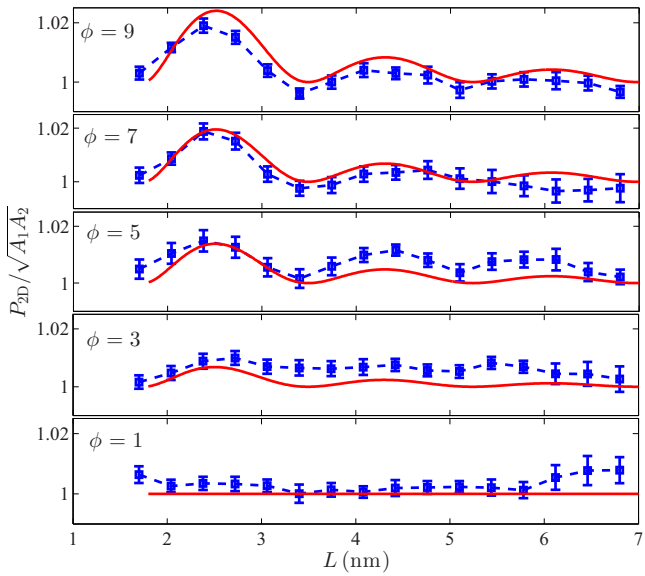

FIG. 11. The length dependent of the ratio of $P_{2D}/\sqrt{A_1A_2}$ for $C = 100$ nm, $P_{3D} = 50$ nm, and different values of ϕ, as indicated. Squares (blue) are the simulation results. (Dashed curves serve as guides for the eye.) and solid lines (red) are our theoretical predictions from Eq. (14) and taking an average over ψ_0.

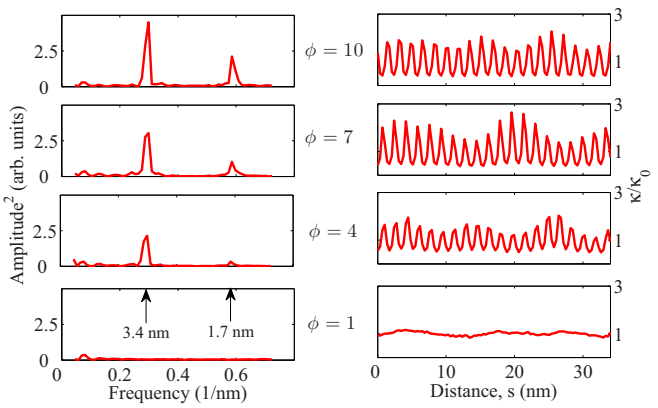

FIG. 12. Right: The normalized curvature, $\kappa(s)/\kappa_0$ (with $\kappa_0 = 2\pi/L$), of the averaged configuration of a two-dimensional anisotropic loop at room temperature. The data correspond to $L = 34$ nm, $C = 100$ nm, $P_{3D} = 50$ nm, and different values of ϕ, as indicated. Left: Fourier spectra of the curvature profile. The arrows indicate the two main periodic components of the curvature.

ground-state conformation of a bent and twisted anisotropic chain [71,72]. We performed MC simulations for a loop with $L = 34$ nm, $C = 100$ nm, $P_{3D} = 50$ nm, and different values of $\phi = 1, 4, 7$, and 10. As the right column of Fig. 12 shows, the curvature along the loop is not uniform, and it is localized with a periodic arrangement (which leads to the transient curvature increasing). In order to visualizing the oscillations during the simulations, we aligned the configurations in the following way: the Fourier spectrum of each snapshot is calculated, then we have taken an average over Fourier transforms, and finally the averaged oscillations in curvature have been constructed by inverse transform. The Fourier spectrum of the curvature reveals two main periodic components, with helical ($2\pi/\omega_0 \simeq 3.4$ nm) and half helical ($\pi/\omega_0 \simeq 1.7$ nm) periods (the two arrows in Fig. 12). This half helical-pitch periodicity is a result of the anisotropic model and vanishes at the isotropic model (i.e., $\phi = 1$). The amplitude of this component increases by increasing the strength of the anisotropy, ϕ.

D. Contribution of bending anisotropy in 2D persistence length of dsDNA

Sequence dependence and bending anisotropy of dsDNA has been widely noticed in base-pair steps approaches, by partitioning the DNA deformation energy through six local variables, slide, shift, rise, tilt, roll, and twist [73]. The rigidity parameters corresponding to these six variables are extracted from their standard deviation as [40]

$$A_i = \frac{k_B T}{\sigma_i^2}, \tag{23}$$

where σ denote the standard deviation and the index i refers to the six local variables. Therefore, the ratio of bending rigidities, ϕ, can be determined by [74]

$$\phi = (\sigma_{\text{roll}}/\sigma_{\text{tilt}})^2. \tag{24}$$

A survey of the values of ϕ obtained by different techniques is presented in Table II. Some of papers cited in this table explicitly report the values of stiffness or standard deviation of the two variables. But in some cases, they present only the distributions of roll and tilt (shown by an asterisk), and we calculate their standard deviations. Despite the diversity, the average value of ϕ from Table II is 2.5 ± 0.2.

TABLE II. Some reported values of ϕ measured by different techniques.

Investigators	ϕ	Method	Ref.
Zhurkin *et al.* (1991)	2–4[a]	MC[c]	[75]
Olson *et al.* (1998)	1–5	XRC[d]	[40]
El Hassan and Calladine (1997)	∼4[b]	XRC	[76]
Richmond *et al.* (2003)	∼2[b]	XRC	[41]
Chua *et al.* (2012)	2–4[b]	XRC	[77]
Stefl *et al.* (2004)	∼3[b]	NMR[e]	[78]
Dornberger *et al.* (1998)	∼2[b]	NMR	[79]
Lankas *et al.* (2000)	∼2	MD[f]	[46]
Lankas *et al.* (2003)	∼2	MD	[80]
Lankas *et al.* (2009)	∼3	MD	[81]
Lankas *et al.* (2010)	2–3[b]	MD and NMR	[42]
Bishop (2005)	1.56	MD	[43]
Lavery *et al.* (2009)	∼2.5[a]	MD	[47]
Perez *et al.* (2005)	∼2	MD	[82]
Perez *et al.* (2008)	∼2	MD	[49]
Becker and Everaers (2007)	1.8	MD	[58]
Teng and Hwang (2015)	2–6	MD	[50]
Balasubramanian *et al.* (2009)	∼2[a]	NAD[g]	[84]

[a] ϕ calculated from the standard deviations and Eq. (24).
[b] Standard deviations calculated from distribution functions.
[c] Monte Carlo simulations.
[d] X-ray crystallography of protein-DNA complexes.
[e] Nuclear magnetic resonance spectroscopy.
[f] All-atom molecular dynamic simulations.
[g] Nucleic Acid Database [83].

For B-DNA the twist rigidity C is in the range 40–110 nm [85,86]. Therefore, the relation between P_{2D}/P_{3D} and ϕ can be written as

$$\frac{P_{2D}}{P_{3D}} = \frac{\phi + 1}{\sqrt{4\phi}}, \tag{25}$$

which is valid for $C \gtrsim 30$ nm (see Sec. III A). By putting $\phi = 2.5 \pm 0.2$ into Eq. (25) we obtain $P_{2D}/P_{3D} = 1.11 \pm 0.02$, which means, due to the bending anisotropy, the persistence length of dsDNA in two dimensions should be about $11 \pm 2\%$ greater than in three dimensions. On the other hand, based on Fig, 1 the average values for P_{2D} and P_{3D} are given by 55.8 ± 3.5 and 43.3 ± 3.7 nm, respectively ($P_{2D}/P_{3D} = 1.29 \pm 0.19$). It can be deduced that with the stiffening of dsDNA the bending anisotropy is partially caused to increase the DNA persistence length in two dimensions (about 10%), while the other effects, such as the excluded volume interactions, different role of divalent ions, and experimental artifacts (e.g., the errors in contour estimation and perturbation during air drying), significantly contribute to the overestimated P_{2D}.

IV. CONCLUSIONS

In summery, we have shown that enforcing the chain into a 2D conformation increases its stiffness. Our analytical approach and MC simulations showed that due to a twist-bend

coupling in the 2D anisotropic model, the effective persistence length depends on the twist rigidity and soon reaches its maximum value when $C \gtrsim 30$ nm. In this limit, the 2D persistence length is given by the geometric mean of the hard and soft bending rigidities, instead of the harmonic mean in three dimensions. In addition, we show that the twist-bend coupling leads to the formation of transient kinks along a curved chain as previously predicted using the energy minimization treatment [71,72].

By taking an average over data reported in the literature we found the average bending anisotropy of dsDNA, and it turns out that the hard bending rigidity is almost 2.5 times larger than the soft bending rigidity. We showed that this bending anisotropy leads to about a 10% increasing 2D persistence length of dsDNA than the 3D one. However, we expect that this estimation is sensitive to the experimental conditions and other effects, such as the excluded volume interactions, divalent ions, and experimental artifacts (e.g., the error in contour estimation and perturbation during air drying). Our analytical procedure can be used as a way to estimate the bending rigidities of other anisotropic bending polymers, such as nanoribbons and dsRNA.

ACKNOWLEDGMENT

We thank the Center of Excellence in Complex Systems and Condensed Matter (CSCM) for partial support.

[1] P. Benetatos and E. Frey, Depinning of semiflexible polymers, Phys. Rev. E **67**, 051108 (2003).
[2] M. D. Wang, H. Yin, R. Landick, J. Gelles, and S. M. Block, Stretching DNA with optical tweezers, Biophys. J. **72**, 1335 (1997).
[3] C. G. Baumann, S. B. Smith, V. A. Bloomfield, and C. Bustamante, Ionic effects on the elasticity of single DNA molecules, Proc. Natl. Acad. Sci. USA **94**, 6185 (1997).
[4] A. Brunet, C. Tardin, L. Salomé, P. Rousseau, N. Destainville, and M. Manghi, Dependence of DNA persistence length on ionic strength of solutions with monovalent and divalent salts: A joint theory-experiment study, Macromolecules **48**, 3641 (2015).
[5] D. Porschke, Persistence length and bending dynamics of DNA from electrooptical measurements at high salt concentrations, Biophys. Chem. **40**, 169 (1991).
[6] W. H. Taylor and P. J. Hagerman, Application of the method of phage T4 DNA ligase-catalyzed ring-closure to the study of DNA structure. II. NaCl-dependence of DNA flexibility and helical repeat, J. Mol. Biol. **212**, 363 (1990).
[7] V. Cassina, M. Manghi, D. Salerno, A. Tempestini, V. Iadarola, L. Nardo, S. Brioschi, and F. Mantegazza, Effects of cytosine methylation on DNA morphology: An atomic force microscopy study, Biochim. Biophys. Acta Gen. Subj. **1860**, 1 (2016).
[8] A. Japaridze, A. Benke, S. Renevey, C. Benadiba, and G. Dietler, Influence of DNA binding dyes on bare DNA structure studied with atomic force microscopy, Macromolecules **48**, 1860 (2015).
[9] B. Kundukad, J. Yan, and P. S. Doyle, Effect of YOYO-1 on the mechanical properties of DNA, Soft Matter **10**, 9721 (2014).
[10] Y. Lu, B. Weers, and N. C. Stellwagen, DNA persistence length revisited, Biopolymers **61**, 261 (2001).
[11] A. K. Mazur and M. Maaloum, Atomic force microscopy study of DNA flexibility on short length scales: Smooth bending versus kinking, Nucleic Acid Res. **42**, 14006 (2014).
[12] J. Moukhtar, E. Fontaine, C. Faivre-Moskalenko, and A. Arneodo, Probing Persistence in DNA Curvature Properties with Atomic Force Microscopy, Phys. Rev. Lett. **98**, 178101 (2007).
[13] A. Podestà, M. Indrieri, D. Brogioli, G. S. Manning, P. Milani, R. Guerra, L. Finzi, and D. Dunlap, Positively charged surfaces increase the flexibility of DNA, Biophys. J. **89**, 2558 (2005).
[14] D. Porschke, Structure and dynamics of double helices in solution: Modes of DNA bending, J. Biomol. Struct. Dyn. **4**, 373 (1986).
[15] C. Rivetti, M. Guthold, and C. Bustamante, Scanning force microscopy of DNA deposited onto mica: Equilibration versus kinetic trapping studied by statistical polymer chain analysis, J. Mol. Biol. **264**, 919 (1996).
[16] P. A. Wiggins, T. van der Heijden, F. Moreno-Herrero, A. Spakowitz, R. Phillips, J. Widom, C. Dekker, and P. C. Nelson, High flexibility of DNA on short length scales probed by atomic force microscopy, Nat. Nanotechnol. **1**, 137 (2006).
[17] A. V. Drozdetski, I. S. Tolokh, L. Pollack, N. Baker, and A. V. Onufriev, Opposing Effects of Multivalent Ions on the Flexibility of DNA and RNA, Phys. Rev. Lett. **117**, 028101 (2016).
[18] S. Geggier and A. Vologodskii, Sequence dependence of DNA bending rigidity, Proc. Natl. Acad. Sci. USA **107**, 15421 (2010).
[19] A. Fathizadeh, B. Eslami-Mossallam, and M. Ejtehadi, Definition of the persistence length in the coarse-grained models of DNA elasticity, Phys. Rev. E **86**, 051907 (2012).
[20] A. Noy and R. Golestanian, Length Scale Dependence of DNA Mechanical Properties, Phys. Rev. Lett. **109**, 228101 (2012).
[21] H. Salari, B. Eslami-Mossallam, M. S. Naderi, and M. R. Ejtehadi, Extreme bendability of DNA double helix due to bending asymmetry, J. Chem. Phys. **143**, 104904 (2015).
[22] V. Rizzo and J. Schellman, Flow dichroism of T7 DNA as a function of salt concentration, Biopolymers **20**, 2143 (1981).
[23] D. Pastré, O. Piétrement, S. Fusil, F. Landousy, J. Jeusset, M.-O. David, L. Hamon, E. Le Cam, and A. Zozime, Adsorption of DNA to mica mediated by divalent counterions: A theoretical and experimental study, Biophys. J. **85**, 2507 (2003).
[24] J. A. Abels, F. Moreno-Herrero, T. van der Heijden, C. Dekker, and N. H. Dekker, Single-molecule measurements of the persistence length of double-stranded RNA, Biophys. J. **88**, 2737 (2005).
[25] J. van Noort, S. Verbrugge, N. Goosen, C. Dekker, and R. T. Dame, Dual architectural roles of HU: Formation of flexible hinges and rigid filaments, Proc. Natl. Acad. Sci. USA **101**, 6969 (2004).
[26] S. Smith, L. Finzi, and C. Bustamante, Direct mechanical measurements of the elasticity of single DNA molecules by using magnetic beads, Science **258**, 1122 (1992).
[27] E. Nordmeier, Absorption-spectroscopy and dynamic and static light-scattering-studies of ethidium-bromide binding to calf thymus DNA: Implications for outside binding and intercalation, J. Phys. Chem. **96**, 6045 (1992).

[28] Z. Kam, N. Borochov, and H. Eisenberg, Dependence of laser light scattering of DNA on NaCl concentration, Biopolymers **20**, 2671 (1981).

[29] J. Bednar, P. Furrer, V. Katritch, A. Z. Stasiak, J. Dubochet, and A. Stasiak, Determination of DNA persistence length by cryo-electron microscopy. Separation of the static and dynamic contributions to the apparent persistence length of DNA, J. Mol. Biol. **254**, 579 (1995).

[30] S. Mantelli, P. Muller, S. Harlepp, and M. Maaloum, Conformational analysis and estimation of the persistence length of DNA using atomic force microscopy in solution, Soft Matter **7**, 3412 (2011).

[31] F. Drube, K. Alim, G. Witz, G. Dietler, and E. Frey, Excluded volume effects on semiflexible ring polymers, Nano Lett. **10**, 1445 (2010).

[32] H.-P. Hsu and K. Binder, Stretching semiflexible polymer chains: Evidence for the importance of excluded volume effects from Monte Carlo simulation, J. Chem. Phys. **136**, 024901 (2012).

[33] H. G. Hansma, I. Revenko, K. Kim, and D. E. Laney, Atomic force microscopy of long and short double-stranded, single-stranded and triple-stranded nucleic acids, Nucleic Acids Res. **24**, 713 (1996).

[34] A. Japaridze, D. Vobornik, E. Lipiec, A. Cerreta, J. Szczerbinski, R. Zenobi, and G. Dietler, Toward an effective control of DNA's submolecular conformation on a surface, Macromolecules **49**, 643 (2016).

[35] C. Rivetti and S. Codeluppi, Accurate length determination of DNA molecules visualized by atomic force microscopy: Evidence for a partial B- to A-form transition on mica, Ultramicroscopy **87**, 55 (2001).

[36] J. T. Waters, X.-J. Lu, R. Galindo-Murillo, J. C. Gumbart, H. D. Kim, T. E. Cheatham, and S. C. Harvey, Transitions of double-stranded DNA between the A- and B-forms, J. Phys. Chem. B **120**, 8449 (2016).

[37] H. Wang and J. N. Milstein, Simulation assisted analysis of the intrinsic stiffness for short DNA molecules imaged with scanning atomic force microscopy, PLoS One **10**, e0142277 (2015).

[38] N. B. Ulyanov and V. B. Zhurkin, Sequence-dependent anisotropic flexibility of B-DNA. A conformational study, J. Biomol. Struct. Dyn. **2**, 361 (1984).

[39] L. Saiz, J. M. Rubi, and J. M. G. Vilar, Inferring the in vivo looping properties of DNA, Proc. Natl. Acad. Sci. USA **102**, 17642 (2005).

[40] W. K. Olson, A. A. Gorin, X. J. Lu, L. M. Hock, and V. B. Zhurkin, DNA sequence-dependent deformability deduced from protein-DNA crystal complexes, Proc. Natl. Acad. Sci. USA **95**, 11163 (1998).

[41] T. J. Richmond and C. A. Davey, The structure of DNA in the nucleosome core, Nature (London) **423**, 145 (2003).

[42] F. Lankaš, N. Špačková, M. Moakher, P. Enkhbayar, and J. Šponer, A measure of bending in nucleic acids structures applied to A-tract DNA, Nucleic Acids Res. **38**, 3414 (2010).

[43] T. C. Bishop, Molecular dynamics simulations of a nucleosome and free DNA, J. Biomol. Struct. Dyn. **22**, 673 (2005).

[44] T. Dršata and F. Lankaš, Multiscale modeling of DNA mechanics, J. Phys.: Condens. Matter **27**, 323102 (2015).

[45] F. Lankas, R. Lavery, and J. H. Maddocks, Kinking occurs during molecular dynamics simulations of small DNA minicircles, Structure **14**, 1527 (2006).

[46] F. Lankas, J. Sponer, P. Hobza, and J. Langowski, Sequence-dependent elastic properties of DNA, J. Mol. Biol. **299**, 695 (2000).

[47] R. Lavery, K. Zakrzewska, D. Beveridge, T. C. Bishop, D. A. Case, T. Cheatham, S. Dixit, B. Jayaram, F. Lankas, C. Laughton, J. H. Maddocks, A. Michon, R. Osman, M. Orozco, A. Perez, T. Singh, N. Spackova, and J. Sponer, A systematic molecular dynamics study of nearest-neighbor effects on base pair and base pair step conformations and fluctuations in B-DNA, Nucleic Acids Res. **38**, 299 (2009).

[48] N. Ma and A. van der Vaart, Anisotropy of B-DNA groove bending, J. Am. Chem. Soc. **138**, 9951 (2016).

[49] A. Perez, F. Lankas, F. J. Luque, and M. Orozco, Towards a molecular dynamics consensus view of B-DNA flexibility, Nucleic Acids Res. **36**, 2379 (2008).

[50] X. Teng and W. Hwang, Elastic energy partitioning in DNA deformation and binding to proteins, ACS Nano **10**, 170 (2016).

[51] K. Alim and E. Frey, Fluctuating semiflexible polymer ribbon constrained to a ring, Eur. Phys. J. E **24**, 185 (2007).

[52] A. Balaeff, L. Mahadevan, and K. Schulten, Elastic Rod Model of a DNA Loop in the *Lac* Operon, Phys. Rev. Lett. **83**, 4900 (1999).

[53] Y.-C. Cheng, S.-T. Feng, and K. Hu, Stability of anisotropic, naturally straight, helical elastic thin rods, Math. Mech. Solids, 1081286516657856 (2016).

[54] B. Eslami-Mossallam and M. R. Ejtehadi, Stretching an anisotropic DNA, J. Chem. Phys. **128**, 125106 (2008).

[55] J.-H. Jeon and W. Sung, An effective mesoscopic model of double-stranded DNA, J. Biol. Phys. **40**, 1 (2014).

[56] D. Norouzi, F. Mohammad-Rafiee, and R. Golestanian, Effect of Bending Anisotropy on the 3D Conformation of Short DNA Loops, Phys. Rev. Lett. **101**, 168103 (2008).

[57] V. B. Zhurkin, Y. P. Lysov, and V. I. Ivanov, Anisotropic flexibility of DNA and the nucleosomal structure, Nucleic Acids Res. **6**, 1081 (1979).

[58] N. B. Becker and R. Everaers, From rigid base pairs to semiflexible polymers: Coarse-graining DNA, Phys. Rev. E **76**, 021923 (2007).

[59] A. Kosmrlj and D. R. Nelson, Response of thermalized ribbons to pulling and bending, Phys. Rev. B **93**, 125431 (2016).

[60] C. Heussinger, M. Bathe, and E. Frey, Statistical Mechanics of Semiflexible Bundles of Wormlike Polymer Chains, Phys. Rev. Lett. **99**, 048101 (2007).

[61] K. Liebl, T. Drsata, F. Lankas, J. Lipfert, and M. Zacharias, Explaining the striking difference in twist-stretch coupling between DNA and RNA: A comparative molecular dynamics analysis, Nucleic Acids Res. **43**, 10143 (2015).

[62] J. F. Marko and E. D. Sigga, Bending and twisting elasticity of DNA, Macromolecules **27**, 981 (1994).

[63] S. K. Nomidis, W. Vanderlinden, J. Lipfert, and E. Carlon, The effect of twist-bend coupling on the torsional properties of double-stranded DNA, arXiv:1603.00835.

[64] F. G. A. Faas, B. Rieger, L. J. Van Vliet, and D. I. Cherny, DNA deformations near charged surfaces: Electron and atomic force microscopy views, Biophys. J. **97**, 1148 (2009).

[65] B. Maier, U. Seifert, and J. O. Rädler, Elastic response of DNA to external electric fields in two dimensions, Europhys. Lett. **60**, 622 (2007).

[66] J. Curuksu, K. Zakrzewska, and M. Zacharias, Magnitude and direction of DNA bending induced by screw-axis orientation: Influence of sequence, mismatches and abasic sites, Nucleic Acid Res. **36**, 2268 (2008).

[67] P. A. Wiggins, R. Phillips, and P. C. Nelson, Exact theory of kinkable elastic polymers, Phys. Rev. E **71**, 021909 (2005).

[68] M. Zoli, Flexibility of short DNA helices under mechanical stretching, Phys. Chem. Chem. Phys. **18**, 17666 (2016).

[69] J. M. Schurr, Effect of anisotropic bending rigidity and finite twisting rigidity on statistical properties of DNA model filaments, Biopolymers **24**, 1233 (1985).

[70] A. Prasad, Y. Hori, and J. Kondev, Elasticity of semiflexible polymers in two dimensions, Phys. Rev. E **72**, 041918 (2005).

[71] G. Bijani, N. H. Radja, F. Mohammad-Rafiee, and M. R. Ejtehadi, Anisotropic elastic model for short DNA loops, arXiv:cond-mat/0605086.

[72] F. Mohammad-Rafiee and R. Golestanian, The effect of anisotropic bending elasticity on the structure of bent DNA, J. Phys.: Condens. Matter **17**, S1165 (2005).

[73] B. Mergell, M. R. Ejtehadi, and R. Everaers, Modeling DNA structure, elasticity and deformations at the base-pair level, Phys. Rev. E **68**, 021911 (2003).

[74] W. K. Olson, N. L. Marky, R. L. Jernigan, and V. B. Zhurkin, Influence of fluctuations on DNA curvature, J. Mol. Biol. **232**, 530 (1993).

[75] V. B. Zhurkin, N. B. Ulyanov, A. A. Gorin, and R. L. Jernigan, Static and statistical bending of DNA evaluated by Monte Carlo simulations, Proc. Natl. Acad. Sci. USA **88**, 7046 (1991).

[76] M. A. El Hassan and C. R. Calladine, Conformational characteristics of DNA: Empirical classifications and a hypothesis for the conformational behavior of dinucleotide steps, Philos. Trans. R. Soc. A Math. Phys. Eng. Sci. **355**, 43 (1997).

[77] E. Y. D. Chua, D. Vasudevan, G. E. Davey, B. Wu, and C. A. Davey, The mechanics behind DNA sequence-dependent properties of the nucleosome, Nucleic Acids Res. **40**, 6338 (2012).

[78] R. Stefl, H. Wu, and S. Ravindranathan, DNA A-tract bending in three dimensions: Solving the dA4T4 vs. dT4A4 conundrum, Proc. Natl. Acad. Sci. USA **101**, 1177 (2004).

[79] U. Dornberger, J. Flemming, and H. Fritzsche, Structure determination and analysis of helix parameters in the DNA decamer d(CATGGCCATG)2: Comparison of results from NMR and crystallography, J. Mol. Biol. **284**, 1453 (1998).

[80] F. Lankas, J. Sponer, J. Langowski, and T. E. Cheatham, DNA basepair step deformability inferred from molecular dynamics simulations, Biophys. J. **85**, 2872 (2003).

[81] F. Lankas, O. Gonzalez, L. M. Heffler, G. Stoll, M. Moakher, and J. H. Maddocks, On the parametrization of rigid base and basepair models of DNA from molecular dynamics simulations, Phys. Chem. Chem. Phys. **11**, 10565 (2009).

[82] A. Pérez, J. R. Blas, M. Rueda, J. M. López-Bes, X. de la Cruz, and M. Orozco, Exploring the essential dynamics of B-DNA, J. Chem. Theory Comput. **1**, 790 (2005).

[83] H. M. Berman, W. K. Olson, D. L. Beveridge, J. Westbrook, A. Gelbin, T. Demeny, S. H. Hsieh, A. R. Srinivasan, and B. Schneider, The nucleic-acid database: A comprehensive relational database of 3-dimensional structures of nucleic-acids, Biophys. J. **63**, 751 (1992).

[84] S. Balasubramanian, F. Xu, and W. K. Olson, DNA sequence-directed organization of chromatin: Structure-based computational analysis of nucleosome-binding sequences, Biophys. J. **96**, 2245 (2009).

[85] J. Lipfert, J. W. J. Kerssemakers, T. Jager, and N. H. Dekker, Magnetic torque tweezers: Measuring torsional stiffness in DNA and RecA-DNA filaments, Nat. Methods **7**, 977 (2010).

[86] S. Neukirch, Extracting DNA Twist Rigidity from Experimental Supercoiling Data, Phys. Rev. Lett. **93**, 198107 (2004).